Fully Printed, Highly Sensitive Multifunctional Artificial Electronic Whisker Arrays Integrated with Strain and Temperature Sensors

Shingo Harada, Wataru Honda, Takayuki Arie, Seiji Akita, and Kuniharu Takei*

Department of Physics and Electronics, Osaka Prefecture University, Sakai, Osaka 599-8531, Japan

ABSTRACT

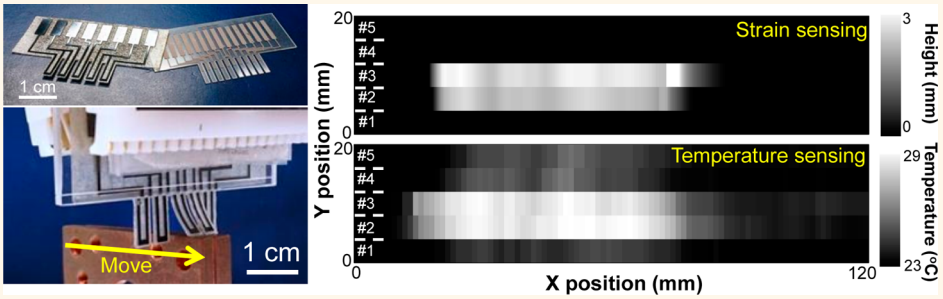

Mammalian-mimicking functional electrical devices have tremendous potential in robotics, wearable and health monitoring systems, and human interfaces. The keys to achieve these devices are (1) highly sensitive sensors, (2) economically fabricated macroscale devices on flexible substrates, and (3) multifunctions beyond mammalian functions. Although highly sensitive artificial electronic devices have been reported, none have been fabricated using cost-effective macroscale printing methods and demonstrate multifunctionalities of artificial electronics. Herein we report fully printed high-sensitivity multifunctional artificial electronic whiskers (e-whisker) integrated with strain and temperature sensors using printable nanocomposite inks. Importantly, changing the composition ratio tunes the sensitivity of strain. Additionally, the printed temperature sensor array can be incorporated with the strain sensor array beyond mammalian whisker functionalities. The sensitivity for the strain sensor is impressively high (~59%/Pa), which is the best sensitivity reported to date (>7× improvement). As the proof-of-concept for a truly printable multifunctional artificial e-whisker array, two- and three-dimensional space and temperature distribution mapping are demonstrated. This fully printable flexible sensor array should be applicable to a wide range of low-cost macroscale electrical applications.

KEYWORDS: printable electronics · artificial whisker · strain sensors · temperature sensors · sensor integrations

The unique sensing functionalities of mammals and insects are attractive for electrical devices and have been aggressively studied. In fact, several approaches have mimicked their functionalities, such as an artificial electronic eye (e-eye),[1] skin (e-skin),[2−8] and nose (e-nose).[9] In addition, an e-whisker has recently been demonstrated using nanomaterial films to detect strain.[10] For practical applications, these kinds of artificial devices must be economically fabricated on macroscale flexible substrates. To date, fully printed macroscale sensor fabrication has yet to be realized, although printing transistors on flexible substrates has been well studied.[11,12] Considering scalability and costs, fully printed artificial devices would be attractive for future electronics.

Herein fully printed, multifunctional highly sensitive e-whisker arrays, which exceed the function of real whiskers, are demonstrated as a proof of concept by developing printing methods and inks to integrate highly sensitive strain and temperature sensors. Although real animal whiskers cannot sense temperature, the temperature distribution is important information if it can be detected prior to touching an object. Thus, a strain sensor to detect whisker displacement and a

* Address correspondence to takei@pe.osakafu-u.ac.jp.

Received for review February 11, 2014 and accepted February 28, 2014.

Published online March 01, 2014
10.1021/nn500845a

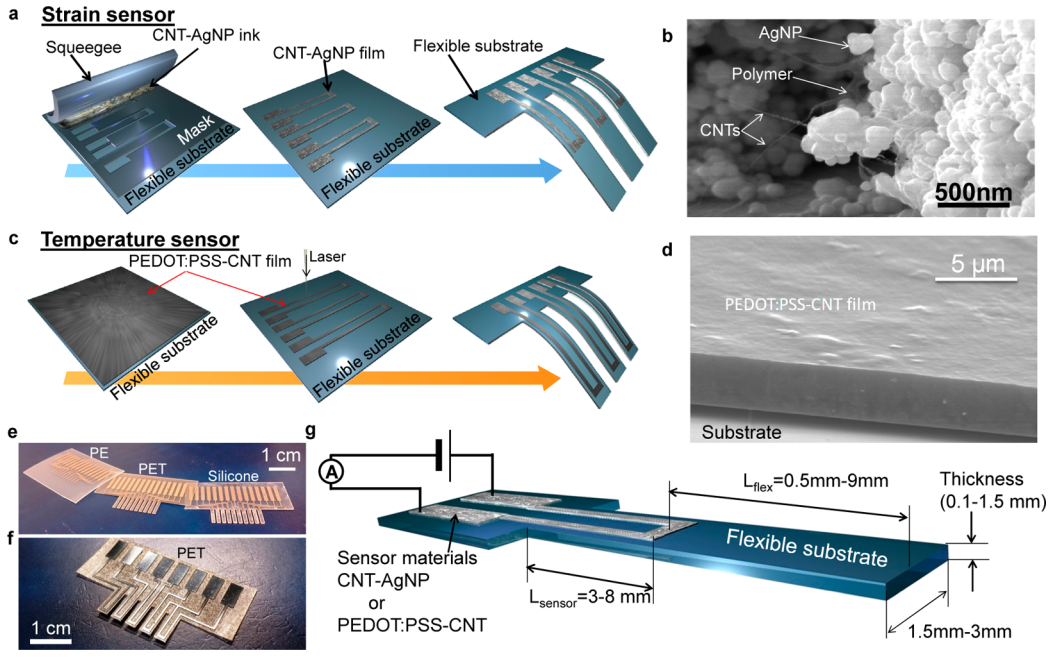

Figure 1. Multifunctional e-whisker fabrication. (a) Schematics to prepare the strain sensor using a screen printer. (b) SEM image of the printed composite CNT-AgNP film (40 wt % AgNP film). (c) Schematics to prepare the temperature sensor using a laser cutter. (d) SEM image of PEDOT:PSS-CNT film (10:1 ratio). Photos of (e) strain sensor arrays printed on a silicone, a PET, and a PE and (f) temperature sensor array on a PET. (g) Device schematics for characterizations.

temperature sensor to detect both an object's and ambient temperature are integrated into the whisker structures.

RESULTS AND DISCUSSION

Figure 1 describes the printing methods for the strain sensor and the temperature sensor array on a plastic substrate (see Methods). Because the sensing materials used here are patterned by the printing method, numerous types of plastic substrates can be used [*e.g.*, silicone, polyethylene terephthalate (PET), and polyethylene (PE)] (Figure 1e,f). Figure 1g describes the design of the sensing material and whisker structure. The structure lengths, L_{flex} and L_{sensor}, and thickness were altered to study the geometric dependence of the strain sensor. The output current was measured to extract stress and temperature.

First, the strain sensor was characterized as shown in Figure 2. The mechanism of the strain sensor using a carbon nanotube (CNT)-silver (Ag) nanoparticle (NP) film is to measure the distance between AgNPs, which corresponds to the resistance as described in Figure 2a. The entangled CNTs connect AgNPs when a high strain is applied to the film. A more detailed sensing mechanism is described elsewhere.[10,13] Although different material systems can be used for the strain sensors (*e.g.*, nanoparticles,[13,14] nanowires,[15,16] and nanotubes[17,18]), this study employs composite materials of nanoparticles and nanotubes because they realize a high sensitivity and wide dynamic range, respectively. Consequently, the composite films display both characteristics.[10] Figure 2b indicates the design to characterize the strain sensor on the whisker structure. The length, L_{flex} (5, 7, and 9 mm), and the thickness of silicone substrates (0.5, 1, and 1.5 mm) were altered, while the length, L_{sensor}, of the CNT-AgNP resistance was fixed at 3 mm.

To determine the highest sensitivity of the fully printed CNT-AgNP film, the composite ratios of the CNT paste and AgNP ink were studied. Figure 2c shows the resistance change as functions of the displacement of a tip of e-whisker and the pressure with different ratios of CNT paste and AgNP ink, where R_0 and R are the resistances at the relaxed state of the e-whisker (*i.e.*, no bending) and at bent state, respectively. The reading increases or decreases in accordance with the bending direction [downward (tensile stress) or upward (compressive stress), respectively]. Figure 2d compiles the normalized resistance change, $\Delta R(= R - R_0)/R_0$, as a function of the AgNP ink ratio in the composite ink when the whisker is bent downward ~2.5 mm to apply a tensile stress in the sensor. Initially increasing the AgNP ratio in the CNT ink drastically increases the resistance as a function of bending, which peaks at 45 wt % AgNP ink (or CNT paste:AgNP ink = 10:8). The 45 wt % AgNP film shows the highest resistance change ~4500% at an applied pressure ~450 Pa (saturation region) and ~2018% at ~34 Pa (linear region), corresponding to a sensitivity ~10%/Pa and ~59%/Pa, respectively. This ~59%/Pa sensitivity is more than seven times higher than the best reported sensitivity (~8%/Pa)[10] for a strain sensor, including sensors composed of a silicon cantilever[19] or other materials.[8,20] However, further increasing the AgNP ratio decreases the resistance change (*e.g.*, AgNP ink

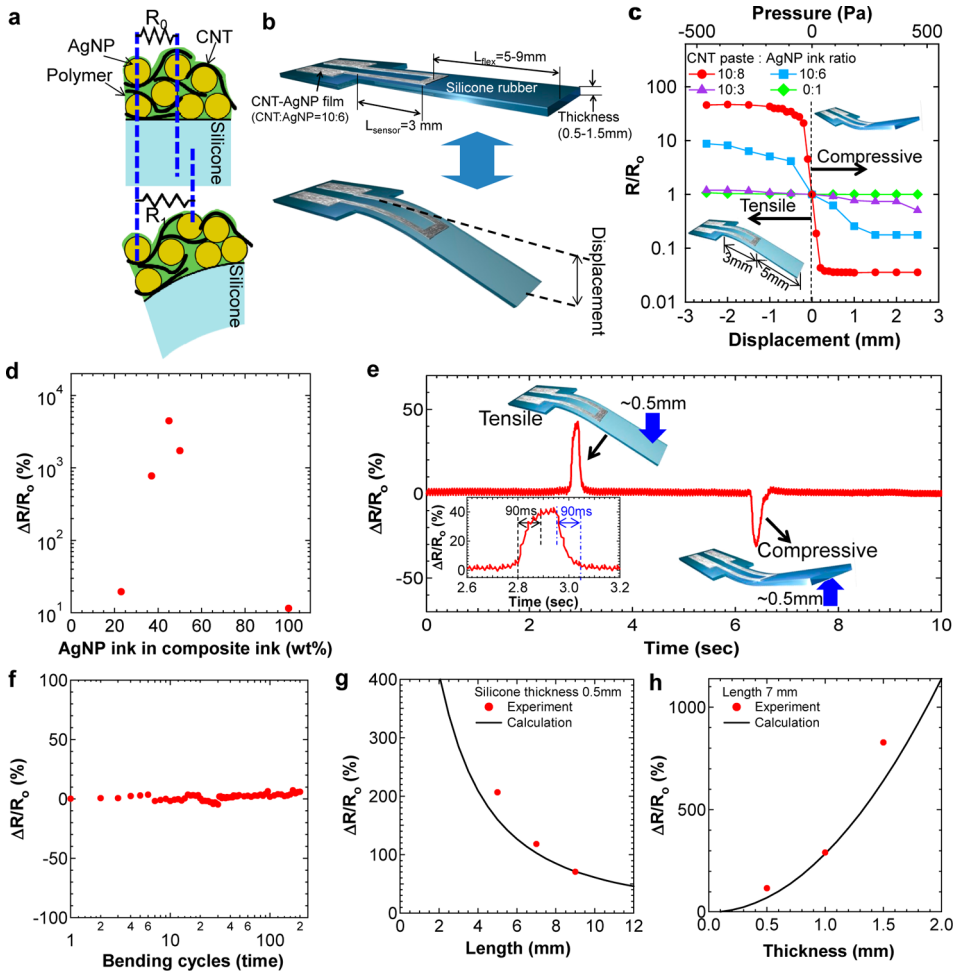

Figure 2. Strain sensors on the e-whisker structure. (a) Schematics of the strain sensing mechanism. (b) Schematics of the strain sensor design and displacement. (c) Resistance change, R/R_0, as functions of displacement (bottom *x*-axis) and applied pressure (top *x*-axis) with different CNT and AgNP ratios. (d) Normalized resistance difference, $\Delta R/R_0$, of the tensile stress as a function of the AgNP ink ratio in the composite ink. (e) Time response of the e-whisker applied tensile and compressive strain by bending ~0.5 mm. Inset shows the e-whisker response time of ~90 ms. (f) Mechanical reliability of the normalized resistance change by bending up to 200 cycles. (g) Normalized resistance change with different lengths, L_{flex} = 5, 7, and 9 mm (silicone thickness is 0.5 mm). Solid line indicates the trend of the resistance change due to strain. (h) Normalized resistance change as a function of silicone thicknesses of 0.5, 1, and 1.5 mm (L_{flex} = 7 mm).

or 50 wt % Ag ink are shown in Figure 2d). This behavior is most likely because the AgNPs are completely packed in the film and the change in the distance between AgNPs is negligible when the strain is applied to the AgNPs. In addition, it is speculated that the amount of binding polymer in the CNT paste also plays an important role to achieve a highly sensitive strain sensor based on the results of 50 wt % AgNP film (*i.e.*, less binding polymer), which shows a low sensitivity. Unfortunately, the composite ink with a AgNP ratio >50 wt % started to aggregate and could not be applied to the screen printing method in this study.

Next the response time of the e-whisker was observed by bending ~0.5 mm to apply tensile and compressive stresses. The resistance change is successfully monitored (Figure 2e), depicting that the response time is ~90 ms (inset of Figure 2e), which is sufficient to map the spatial distributions of e-whiskers and robotic applications. This time delay is most likely due to the speed of the silicone elastomer. Thus, the response time may be improved by choosing a different substrate material.

Then the mechanical reliability of the fully printed film was measured by observing the normalized resistance change ($\Delta R(= R - R_0)/R_0$), where R_0 is the initial resistance before bending. Here the resistance R was measured in the relaxed state of e-whisker after bending (~1 mm) up to 200 times. Figure 2f shows that the resistance change is almost negligible, suggesting that printed CNT-AgNP film is mechanically flexible and stable.

To shed further light on the properties of e-whiskers, the geometric dependencies of the length and thickness of e-whiskers were characterized by measuring the normalized resistance change. Because the sensor using 45 wt % AgNP film is too sensitive for a systematic study, the 40 wt % AgNP film is used here. First, the e-whisker length L_{flex} was altered from 5 to 9 mm with a

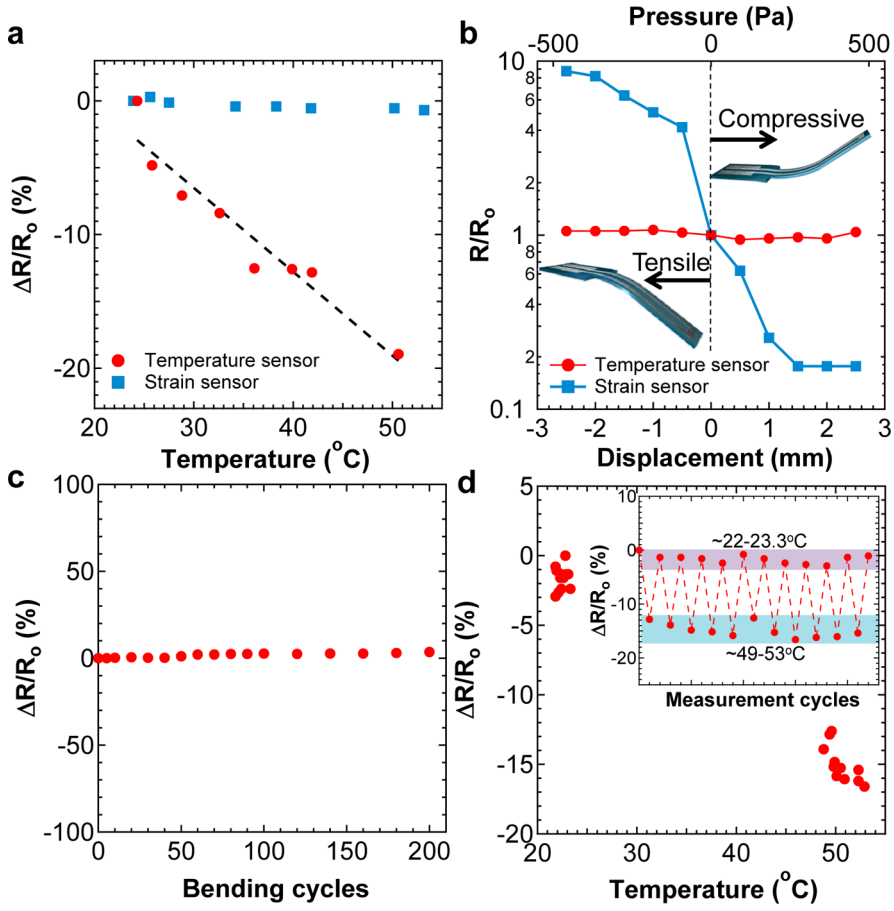

Figure 3. Temperature sensor. (a) Temperature dependence of PEDOT:PSS-CNT and CNT-AgNP film (40 wt % AgNP film). (b) Resistance change as functions of displacement (bottom *x*-axis) and pressure (top *x*-axis) for temperature and strain sensors. (c) Mechanical reliability of the normalized resistance change up to 200 cycle bendings. (d) Repeated cycle test of temperature between R.T. and ~50 °C.

silicone thickness of 0.5 mm and L_{sensor} = 3 mm. The e-whisker was bent ~2 mm, and the resistance change was measured as a function of the whisker length. The trend of the resistance change based on strain by bending the e-whisker can be estimated as a function of length. The surface strain, *S*, can be calculated by the following equation[21]

$$S = \left(\frac{d_t + d_s}{2R}\right)\frac{(1 + 2\eta + \chi\eta^2)}{(1 + \eta)(1 + \chi\eta)}$$

where d_t and d_s are the thicknesses of CNT-AgNP film (~1.5 μm) and silicone substrate (0.5 mm), respectively. *R* is bending radius, $\eta = d_t/d_s$, and χ is the Young modulus ratio of the CNT-AgNP film and silicone. Due to difficulty extracting the Young modulus of the CNT-AgNP film, the exact value of strain cannot be estimated. However, based on the trend of strain with different thicknesses and lengths of the whisker from the above equation, strain corresponding to $\Delta R/R_0$ increases as the length decreases at a constant displacement ~2 mm (Figure 2g). The experimental and calculated results are consistent (Figure 2g). The thickness dependence with L_{flex} = 7 mm and L_{sensor} = 3 mm was also characterized when the e-whisker was bent ~0.5 mm; $\Delta R/R_0$ increases when the thickness of silicone substrate increases. This trend of the resistance change calculated by the strain also agrees well with experimental values as a function of thickness (Figure 2h). These results demonstrate that the properties of the e-whisker structure can be estimated by the fundamental strain theory for a cantilever structure.

In addition to the strain sensor to detect the spatial distribution, a printed resistive temperature sensor was fabricated on the e-whisker to imitate animal skin. The resistance change of the printed poly(3,4-ethylenedioxythiophene)-poly(styrenesulfonate) (PEDOT:PSS)-CNT composite film used in this report is a function of temperature due to the temperature coefficient of each PEDOT:PSS and CNT and electron hopping at the interface of PEDOT:PSS and CNTs.[22] The normalized resistance change [$\Delta R(= R - R_0)/R_0$] where R_0 and *R* are the resistance at room temperature (R.T. ~24.3 °C) and the temperature from 25.8 to 53.2 °C, respectively, was measured. Figure 3a indicates that the resistance decreases as the temperature increases. The sensitivity extracted by the linear fit in Figure 3a is ~0.63%/°C, which is similar or better than the

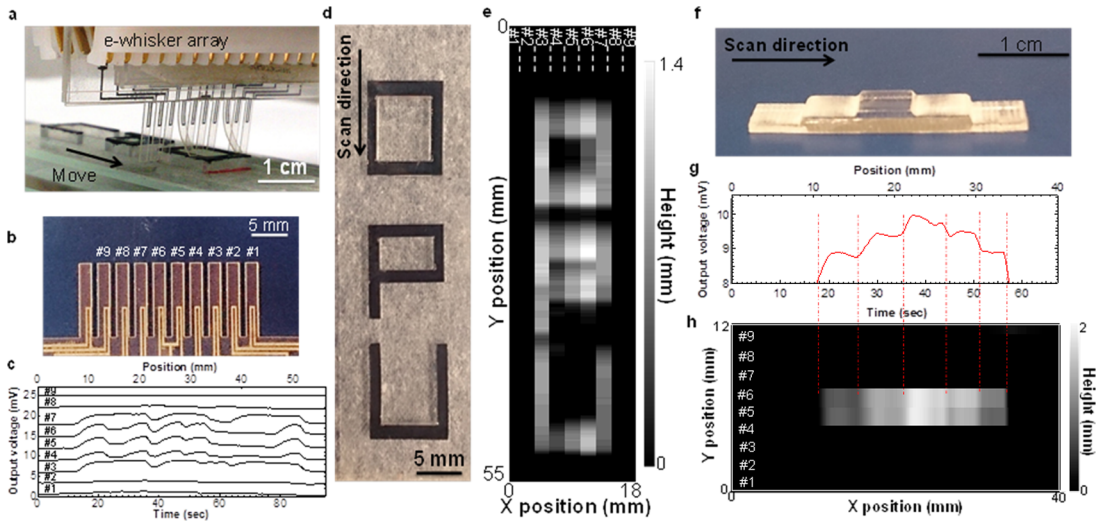

Figure 4. Three-dimensional spatial distribution mapping. Photos of (a) the measurement and (b) 9-e-whisker array used for the mapping. (c) Output voltage of each e-whisker #1−#9. (d) Photo of an object "OPU" for three-dimensional mapping. (e) Three-dimensional mapping result by scanning over "OPU" object shown in (d). Height difference mapping of (f) the stair-like object, (g) output voltage of e-whisker #5, and (h) three-dimensional height mapping.

properties of other temperature sensors fabricated on flexible substrates,[23] although here the temperature sensor was patterned by printing and laser cutting methods. The temperature sensitivity of the strain sensor using the CNT-AgNP film (40 wt % AgNP film) is negligible ~0.03%/°C; that is, it is 20 times lower than that of the temperature sensor plotted in Figure 3a. On the other hand, the responses of the temperature sensor are negligible for both tensile and compressive strains (Figure 3b), whereas the strain sensor shows a large change in resistance. To prevent complicated analyses, these selectivities are important in order to integrate both strain and temperature sensors on e-whiskers.

The mechanical and electrical reliabilities of the temperature sensor were characterized. First, the normalized resistance changes of the same experiment in Figure 2f were evaluated to confirm whether bending the substrate degrades the sensor. Figure 3c shows that the temperature sensor suffers negligible damage or degradation against strain. Subsequently, a cycle test of the temperature difference between ~22−23.3 and ~49−53 °C was carried out to observe the resistance changes due to degradation by temperature of the film. Figure 3d indicates that the sensor operates consistently during different temperature cycle tests, which is essential for flexible devices.

As an e-whisker demonstration, the spatial distribution upon touching an object similar to an animal whisker was experimentally mapped using integrated 9-e-whisker arrays. The e-whisker arrays were connected to a Wheatstone bridge circuit to convert the resistance change into a voltage change. The output voltage simultaneously recorded the 9 channel memory recorder. The sampling rate of the memory recorder was 0.1 s, the input voltage was 1 V, and the scanning speed was 0.6 mm/s. A strain sensor with 40 wt % AgNP film was patterned on a 100-μm-thick PET substrate (sheet resistance at the relaxed state ~120 mΩ/sq). The e-whisker array was simply cramped by an electrical lead-out connector (Figure 4a). The whisker length was 1 cm (L_{flex} = 7 mm and L_{sensor} = 3 mm) (Figure 4b). An object "OPU" with a 1.4-mm height was scanned using the 9-e-whisker array (Figure 4d). Figure 4c shows the recorded electrical signal and the three-dimensional spatial distribution map. Figure 4e confirms that the "OPU" object is successfully mapped out electrically. In addition to the mapping of the same height, height differences should be measured to imitate real animal whiskers. To confirm this capability, a stair-like object as shown in Figure 4f was prepared. Figure 4g,h describes the electrical output, and clearly shows up and down steps with a height difference of ~400 μm. Minimum height resolution depends on the geometry of e-whisker and measurement setups. In this study, the minimum resolution was tens of micrometer due to noise from the measurement environment and amplifiers to detect the voltage change of the sensors. In principle, the height resolution should be improved up to nanometer range based on Figure 2c if the structure is correctly designed and the measurement setup is improved. The printing technique limits the spatial resolution (~2 mm between e-whiskers) because the screen printing was manually conducted. Using automatic full-controlled screen printers or some other printing techniques such as inkjet printers should create high-density patterning to realize high resolution mapping.

As the first proof of concept, the three-dimensional physical space and temperature distributions by integrating strain and temperature sensor arrays on the

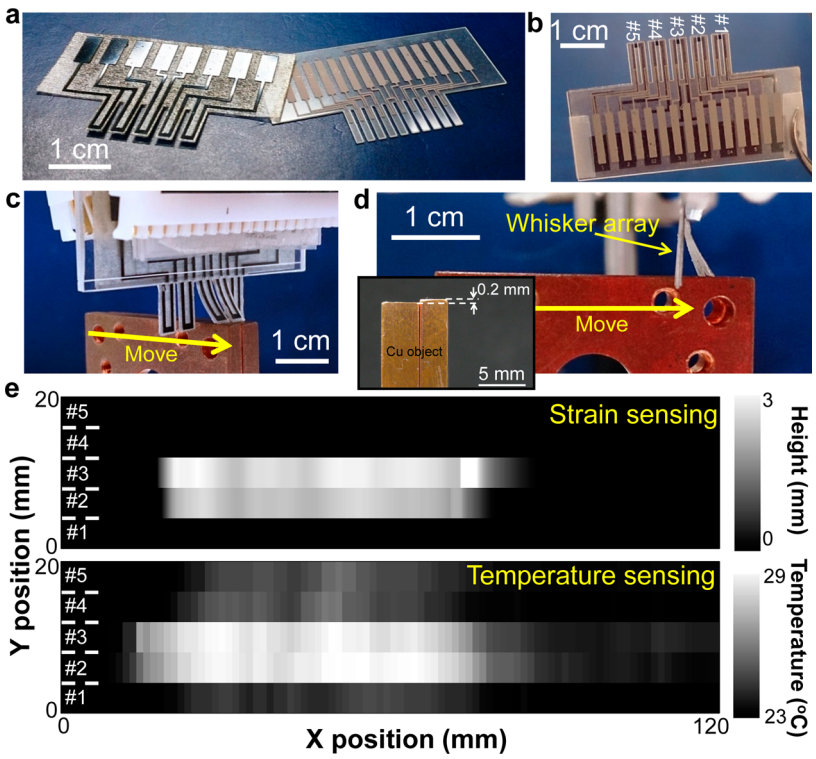

Figure 5. Multifunctional e-whisker array with strain and temperature sensors. Photos of (a) each e-whisker array integrated with temperature and strain sensors on a PET substrate, (b) multifunctional e-whisker array laminated with strain and temperature e-whiskers, and (c and d) measurement setup to scan a copper object. Inset picture shows the height difference ~200 μm of copper plates. (e) Three-dimensional strain and temperature distribution simultaneously mapped by the multifunctional e-whisker array.

e-whiskers were demonstrated (Figure 5a,b). The strain and temperature e-whisker arrays were separately fabricated and then laminated together. A copper object, which consisted of two copper plates, was used to map the shape and temperature distributions (Figure 5c,d). The height of the copper objects between two plates differed slightly (within ~200 μm) (Figure 5d inset). First, the copper object was heated to ~70 °C on a hot plate and placed on the stage of the scanner. The object quickly cooled due to the unheated scanner stage in an air-conditioned room at 24 °C. Multifunctional e-whisker arrays were scanned over the object. Figure 5e shows the height and temperature distributions, suggesting that the multifunctional e-whisker array successfully maps the space and temperature distributions. For temperature mapping, e-whiskers that did not touch the object display a slight temperature change because the e-whiskers also measure small temperature changes from the radiant heat of the copper object. It is noteworthy that the strain sensor (Figure 5e) detects the height difference between e-whiskers #2 and #3 due to ~200 μm height difference of the copper object, confirming that the e-whisker can measure a small height difference of ~200 μm. Since the plastic substrates were used in this study, the substrates start to deform at high temperature above 90 °C. For high temperature measurement, if needed, thermally resistive flexible substrates such as polyimide need to use for both strain and temperature sensors.

CONCLUSIONS

In summary, here a fully printed, multifunctional e-whisker array integrated with strain and temperature sensors is demonstrated. The strain sensor shows an impressively high sensitivity of ~59%/Pa, which is the best value compared to all other previously reported types of strain sensors.[8,10,19,20] In addition, by changing the CNT and AgNP ratio, the sensitivity of the strain sensor is tunable for different applications. Another advantage is that the e-whisker arrays are patterned by conventional standard screen printing, which is readily conducted and reproduced using economic macroscale fabrication techniques. Beyond a real animal whisker, the temperature sensor is also integrated to provide additional information for robotics and artificial skin applications. Finally, the ability of multifunctional e-whisker arrays to successfully map two- and three-dimensional distributions is demonstrated. To realize fully printed flexible electronic system, there are still many challenges such as fabrications of flexible circuits and batteries, protecting layers of devices, and techniques of high integration, which must be realized by printing methods and/or comparable low-cost fabrication methods. These requirements need to address as next research topics in the near future. However, this

fully printed, macroscale multifunctional integrated device should lead fields involving low-cost and high performance electronics, robotics, and similar applications including printable electronics.

METHODS

Strain Sensor Printing. A carbon nanotube (CNT) paste (SWeNT) and silver (Ag) nanoparticle (NP) ink (Paru, Korea) were mixed with a predetermine weight ratio for the strain sensor. The resistance change as a function of strain was measured to define compressive and tensile strains as well as applied pressure. The CNT-AgNP resistive film was printed onto a flexible plastic substrate using a screen printing method (Figure 1a). Oxygen plasma was applied to a silicone rubber substrate for uniform printing. The plastic substrate was then patterned by a laser cutter to form the whisker structure. The film of CNTs entangled around the AgNPs had a total thickness of $\sim$1.5 μm (Figure 1b). The CNT-Ag composite film contained a binding polymer that came from the CNT paste.

Temperature Sensor Printing. A conductive poly(3,4-ethylenedioxythiophene)-poly(styrenesulfonate) (PEDOT:PSS, 1.3 wt % in water) (Sigma-Aldrich) and the same CNT paste as the strain sensor were mixed in a 10:1 weight ratio.[22] The PEDOT:PSS-CNT film was printed on the entire plastic surface with a thickness of $\sim$3 μm. To pattern the temperature sensor, a laser cutter tool was used to etch a PEDOT:PSS-CNT film followed by patterning of the plastic substrate to form the whisker structure. It should be noted that patterning using a laser cutter took <1 min for a 3 $\times$ 3-cm^2 substrate size. Figure 1d, which shows a scanning electron microscope (SEM) image of a PEDOT:PSS-CNT film, indicates that the film is uniformly printed over the substrate.

Conflict of Interest: The authors declare no competing financial interest.

Acknowledgment. This work was partially supported by the Mazda Foundation, the Foundation Advanced Technology Institute (ATI) and JSPS KAKENHI Grant (#25889048).

REFERENCES AND NOTES

1. Song, Y. M.; Xie, Y.; Malyarchuk, V.; Xiao, J.; Jung, I.; Choi, K.-J.; Liu, Z.; Park, H.; Lu, C.; Kim, R.-H.; *et al.* Digital Cameras with Designs Inspired by the Arthropod Eye. *Nature* **2013**, *497*, 95–99.
2. Takei, K.; Takahashi, T.; Ho, J. C.; Ko, H.; Gillies, A. G.; Leu, P. W.; Fearing, R. S.; Javey, A. Nanowire Active-Matrix Circuitry for Low-Voltage Macroscale Artificial Skin. *Nat. Mater.* **2010**, *9*, 821–826.
3. Schwartz, G.; Tee, B. C.-K.; Mei, J.; Appleton, A. L.; Kim, D. H.; Wang, H.; Bao, Z. Flexible Polymer Transistors with High Pressure Sensitivity for Application in Electronic Skin and Health Monitoring. *Nat. Commun.* **2013**, *4*, 185910.1038/ncooms2832.
4. Kim, D.-H.; Lu, N.; Ma, R.; Kim, Y.-S.; Kim, R.-H.; Wang, S.; Wu, J.; Won, S. M.; Tao, H.; Islam, A.; *et al.* Epidermal Electronics. *Science* **2011**, *333*, 838–843.
5. Someya, T.; Sekitani, T.; Iba, S.; Kato, Y.; Kawaguchi, H.; Sakurai, T. A Large-Area, Flexible Pressure Sensor Matrix with Organic Field-Effect Transistors for Artificial Skin Applications. *Proc. Natl. Acad. Sci. U.S.A.* **2004**, *101*, 9966–9970.
6. Wu, W.; Wen, X.; Wang, Z. L. Taxel-Addressable Matrix of Vertical-Nanowire Piezotronic Transistors for Active and Adaptive Tactile Imaging. *Science* **2013**, *340*, 952–957.
7. Wang, C.; Hwang, D.; Yu, Z.; Takei, K.; Park, J.; Chen, T.; Ma, B.; Javey, A. User-Interactive Electronic Skin for Instantaneous Pressure Visualization. *Nat. Mater.* **2013**, *12*, 899–904.
8. Mannsfeld, S. C. B.; Tee, B. C.-K.; Stoltenberg, R. M.; Chen, C. V. H-H.; Barman, S.; Muir, B. V. O.; Sokolov, A. N.; Reese, C.; Bao, Z. Highly Sensitive Flexible Pressure Sensors with Microstructured Rubber Dielectric Layers. *Nat. Mater.* **2010**, *9*, 859–864.
9. Misawa, N.; Mitsuno, H.; Kanzaki, R.; Takeuchi, S. Highly Sensitive and Selective Odorant Sensor using Living Cells Expressing Insect Olfactory Receptors. *Proc. Natl. Acad. Sci. U.S.A.* **2010**, *107*, 15340–15344.
10. Takei, K.; Yu, Z.; Zheng, M.; Ota, H.; Takahashi, T.; Javey, A. Highly-Sensitive Electronic-Whiskers Based on Patterned Carbon Nanotube and Silver Nanoparticle Composite Films. *Proc. Natl. Acad. Sci. U.S.A.* **2014**, *111*, 1703–1707.
11. Jung, M.; Kim, J.; Noh, J.; Lim, N.; Lim, C.; Lee, G.; Kim, J.; Kang, H.; Jung, K.; Leonard, A. D.; *et al.* All-Printed and Roll-to-Roll-Printable 13.56-MHz-Operated 1-bit RF Tag on Plastic Foils. *IEEE Trans. Electron Devices* **2010**, *3*, 571–580.
12. Lau, P. H.; Takei, K.; Wang, C.; Ju, Y.; Kim, J.; Yu, Z.; Takahashi, T.; Cho, G.; Javey, A. Fully Printed, High Performance Carbon Nanotube Thin-Film Transistors on Flexible Substrates. *Nano Lett.* **2013**, *13*, 3864–3869.
13. Herrmann, J.; Muller, K.-H.; Reda, T.; Baxter, G. R.; Raguse, B.; de Groot, G. J. J. B.; Chai, R.; Roberts, M.; Wieczorek, L. Nanoparticle Films as Sensitive Strain Gauges. *Appl. Phys. Lett.* **2007**, *91*, 183105.
14. Farcau, C.; Sangeetha, N. M.; Moreira, H.; Viallet, B.; Grisolia, J.; Ciuculescu-Pradines, D.; Ressier, L. High-Sensitivity Strain Gauge Based on a Single Wire of Gold Nanoparticles Fabricated by Stop-and-Go Convective Self-Assembly. *ACS Nano* **2011**, *9*, 7137–7143.
15. Xiao, X.; Yuan, L.; Zhong, J.; Ding, T.; Liu, Y.; Cai, Z.; Rong, Y.; Han, H.; Zhou, J.; Wang, Z. L. High-Strain Sensors Based on ZnO Nanowire/Polystyrene Hybridized Flexible Films. *Adv. Mater.* **2011**, *23*, 5440–5444.
16. Pang, C.; Lee, G.-Y.; Kim, T.-i.; Kim, S. M.; Kim, H. N.; Ahn, S.-H.; Suh, K.-Y. A Flexible and Highly Sensitive Strain-Gauge Sensor Using Reversible Interlocking of Nanofibres. *Nat. Mater.* **2012**, *11*, 795–801.
17. Yamada, T.; Hayamizu, Y.; Yamamoto, Y.; Yomogida, Y.; Izadi-Najafabadi, A.; Futaba, D. N.; Hata, K. A Stretchable Carbon Nanotube Strain Sensor for Human-Motion Detection. *Nat. Nanotechnol.* **2011**, *6*, 296–301.
18. Lipomi, D. J.; Vosgueritchian, M.; Tee, B. C.-K.; Hellstrom, S. L.; Lee, J. A.; Fox, C. H.; Bao, Z. Skin-Like Pressure and Strain Sensors Based on Transparent Elastic Films of Carbon Nanotubes. *Nat. Nanotechnol.* **2011**, *6*, 788–792.
19. Takahashi, H.; Dung, N. M.; Matsumoto, K.; Shimoyama, I. Differential Pressure Sensor Using a Piezoresistive Cantilever. *J. Micromech. Microeng.* **2012**, *22*, 055015.
20. Liu, X.; Zhu, Y.; Nomani, M. W.; Wen, X.; Hsia, T.-Y.; Koley, G. A Highly Sensitive Pressure Sensor Using a Au-Patterned Polydimethylsiloxane Membrane for Biosensing Applications. *J. Micromech. Microeng.* **2013**, *23*, 025022.
21. Suo, Z.; Ma, E. Y.; Gleskova, H.; Wagner, S. Mechanics of Rollable and Foldable Film-on-Foil Electronics. *Appl. Phys. Lett.* **1999**, *74*, 1177–1179.
22. Honda, W.; Harada, S.; Arie, T.; Akita, S.; Takei, K. Wearable, Human-Interactive, Health-Monitoring Wireless Devices Fabricated by Macroscale Printing Techniques. *Adv. Funct. Mater.* **2014**, 10.1002/adfm.201303874.
23. Kim, D.-H.; Lu, N.; Ghaffari, R.; Kim, Y.-S.; Lee, S. P.; Xu, L.; Wu, J.; Kim, R.-H.; Song, J.; Liu, Z.; *et al.* Materials for Multifunctional Ballon Catheters with Capabilities in Cardiac Electrophysiological Mapping and Ablation Therapy. *Nat. Mater.* **2011**, *10*, 316–323.